Composition dependence of exchange stiffness in Fe_xPt_{1-x} alloys

C. Antoniak,[1] J. Lindner,[1] K. Fauth,[2] J.-U. Thiele,[3] J. Minár,[4] S. Mankovsky,[4] H. Ebert,[4] H. Wende,[1] and M. Farle[1]
[1]*Fakultät für Physik and Center for Nanointegration Duisburg-Essen (CeNIDE), Universität Duisburg-Essen, Lotharstr. 1, D-47048 Duisburg, Germany*
[2]*Experimentelle Physik IV, Universität Würzburg, Am Hubland, D-97074 Würzburg, Germany*
[3]*Research and Technology Development, Seagate Technology, 47010 Kato Road, Fremont, California 94538, USA*
[4]*Department Chemie und Biochemie, Ludwig-Maximilians-Universität München, Butenandtstr. 11, D-81377 München, Germany*
(Received 18 March 2010; revised manuscript received 5 July 2010; published 4 August 2010)

The exchange stiffness constants of chemically disordered Fe_xPt_{1-x} films with thickness around 50 nm were determined by means of ferromagnetic resonance. It was found to increase with increasing Fe content from 6 ± 4 pJ/m for $x=0.27$ to 15 ± 4 pJ/m for $x=0.67$. Theoretical results from fully relativistic and scalar-relativistic band-structure calculations using the Korringa-Kohn-Rostoker method confirm the experimentally obtained values. In addition, determination of the magnetocrystalline anisotropy by angular-dependent measurements of the ferromagnetic resonance gave the possibility to estimate the exchange length that was found to be 40–50 nm for all compositions investigated in this work.

DOI: 10.1103/PhysRevB.82.064403 PACS number(s): 76.50.+g, 71.70.Gm, 75.30.Gw

I. INTRODUCTION

The systematic investigation of spin waves and exchange stiffness gives the possibility, e.g., to gain more insight into spin torque and domain-wall (de)pinning which are recently discussed intensively especially relating to new magnetologic or data storage devices. For example, the recently presented domain-wall logic[1] uses the magnetic domain wall in nanowires made of soft-magnetic materials like Permalloy as transition edge in a changing signal. However, reducing the dimensionality of such components to the nanometer scale leads to the FePt system as a promising candidate[2] with its high magnetocrystalline anisotropy in the chemically ordered state to avoid thermally activated fluctuations of the magnetic moments, the so-called superparamagnetism,[3] as discussed in the literature.

The intense research activities on nanoparticles of Fe_xPt_{1-x} alloys over the last decades did not only lead to new results on the structural and magnetic properties (see, e.g., Refs. 4–8) but also reveals some lack of knowledge about the bulk system. Driven by the on-going discussion about spin canting effects that may occur in Fe_xPt_{1-x} nanoparticles,[9–11] we examined the exchange stiffness in the corresponding bulk material which is connected to the length scale of dominating exchange coupling (exchange length) which usually suppresses spin canting. Ferromagnetic resonance (FMR) was used as a powerful tool for the determination of (i) the magnetocrystalline anisotropy by angular-dependent measurements and (ii) the exchange stiffness constant A by the analysis of standing spin waves excited in the material. The results are supported by theoretical calculations using the spin-polarized relativistic Korringa-Kohn-Rostoker (SPR-KKR) method.[12]

II. EXPERIMENTAL DETAILS

Epitaxial Fe_xPt_{1-x} films with thickness around 50 nm were grown on MgO(001) substrates at room temperature by magnetron cosputtering from Fe and Pt targets in a vacuum system with a base pressure of about 10^{-6} Pa. The deposition rate was about 0.1 nm/s. X-ray diffraction indicates a high degree of structural order, the mosaic spread is below 1°. The layer thickness determined by Rutherford backscattering was found to be 46 ± 6 nm and therefore, the films are expected to exhibit bulk properties.

Room-temperature FMR experiments were performed using a constant microwave frequency of $\nu\approx10$ GHz with a power of $P\approx5$ mW. The sample was centered in a cylindric microwave cavity operated in the TE_{011} mode and a quasistatic external magnetic field was swept up to $\mu_0 H_{ext}=1.8$ T. For this setup, the magnetic part of the microwave coupled into the cavity is maximum in the center of the cavity and aligned parallel to the axis of rotational symmetry of the cylindric cavity which is perpendicular to the external quasistatic magnetic field. The electric field component of the microwave vanishes in the center of the cavity. However, a sample with finite dimensions may short the electric field lines off-center. In order to minimize these effects, the sample was cut into small pieces, about 2×2 mm^2. For this size, also inhomogeneities of the magnetic field component are negligible. In general, microwave absorption of the sample can be detected if the precession frequency of magnetization equals the frequency of the irradiated microwave. In the ground state of the system, all spins of a ferromagnet are aligned parallel due to the exchange interaction while precessing around the effective magnetic field $\vec{H}_{eff}$ consisting of the external magnetic field, anisotropy fields, exchange field, and the magnetic component of the microwave. This is the so-called *uniform mode* of precession.

Spin waves (magnons) may be excited by the microwave. A schematic example of a spin wave is shown in Fig. 1. In this case, the effective magnetic field is parallel to the z direction and the spin wave propagates along the y direction. All magnetic moments precess around the field direction including the same angle β but with a constant angular difference α between neighboring moments. Additional surface or interface pinning of the spins may lead to the occurrence of standing spin waves. In the case of a magnetic field pointing

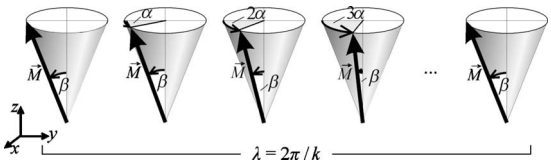

FIG. 1. Example of a spin wave propagating along the y direction while the effective field is parallel to the z direction.

along the sample normal, their possible wave vectors are given by the condition $k_n = n\pi/t$, where t denotes the sample thickness. For small β and small α, the frequency of the precession around the exchange field can be written as[13]

$$\omega_n = \gamma D k_n^2 = \gamma D \frac{\pi^2}{t^2} n^2, \tag{1}$$

where $\gamma = g\mu_B/\hbar$ is the magnetogyric ratio depending on the spectroscopic splitting factor g and D is the spin-wave stiffness related to the exchange stiffness via $A = \mu_0 M_s D/2$. In a FMR experiment, standing spin waves yield additional resonances H_n shifted relatively to the one of the uniform precession H_{uni},

$$H_n = H_{uni} - \frac{\pi^2 D}{t^2} n^2. \tag{2}$$

In this work, only spin waves with $n=1$ could be observed. For this case, the exchange stiffness can be determined from the experimental data using the following equation:

$$A = \frac{1}{2}\mu_0 M_s (H_{uni} - H_1)\frac{t^2}{\pi^2}. \tag{3}$$

The magnetocrystalline anisotropy as well as the effective magnetization were determined by polar and azimuth angular-dependent measurements at room temperature. Since the anisotropy may strongly depend on the temperature,[14–18] FMR spectra were taken also at 20 K for the sample with the lowest Curie temperature,[19,20] i.e., $Fe_{0.26}Pt_{0.74}$. No shift in the resonance field compared to room temperature measurements was obtained within experimental errors. Therefore, FMR measurements at room temperature seemed to be sufficient for all samples investigated in this work.

III. SPR-KKR CALCULATIONS

Band-structure calculations for chemically disordered Fe_xPt_{1-x} alloys were performed by means of the fully relativistic spin-polarized version of the KKR band-structure method (SPR-KKR) within the framework of spin density-functional theory.[12] As structural input for the SPR-KKR calculations, lattice constants of the single-crystalline Fe_xPt_{1-x} films experimentally investigated in this work were used. The values obtained by x-ray diffraction can be found elsewhere[21] and are in agreement to other values reported in the literature for this system.[22] The SPR-KKR method represents the electronic structure in terms of the Green's function evaluated by means of multiple-scattering theory. This feature allows to deal with the chemical disorder by using the coherent potential approximation alloy theory as done in this work for the chemically disordered Fe_xPt_{1-x} alloys. Spin and angular momentum resolved density of states at the Fe and Pt sites as well as element-specific magnetic moments have been published elsewhere.[21]

In the scalar-relativistic mode, *ab initio* Heisenberg pair exchange parameters were calculated using the formulation of Liechtenstein *et al.*[23] The exchange constant was calculated for all Fe-Fe, Fe-Pt, and Pt-Pt pairs as a function of distance. In the case of dominating exchange coupling between nearest-neighbor atoms, the exchange stiffness can be written in general for a single-element system as[24]

$$A = \frac{JS^2}{a} \approx \frac{J}{ag^2}\frac{\mu_s^2}{\mu_B^2}, \tag{4}$$

where a denotes the lattice constant, J the exchange coupling constant, and S and μ_S the spin moment and the spin magnetic moment, respectively.[25] To achieve higher accuracy, in this work not only nearest-neighbor atoms but contributions from all atoms within a cluster of radius $R=3a$ were included. The values of J for all considered Fe-Fe, Fe-Pt, and Pt-Pt pairs were weighted by their probability and summed up assuming complete chemical disorder. For instance, the probability to find an Fe-Fe pair in an Fe_xPt_{1-x} alloy is $P_{FeFe}=x^2$, an Fe-Pt pair $P_{FePt}=P_{PtFe}=x(1-x)$ and a Pt-Pt pair $P_{PtPt}=(1-x)^2$. Thus J can be written for all nearest-neighbor contributions as $J=x^2J_{FeFe}+2x(1-x)J_{FePt}+(1-x)^2J_{PtPt}$. Since there is a significant difference in the calculated and experimentally determined values of the Fe spin magnetic moment for the Fe-rich alloys, experimental values[21] were taken to determine the value of the exchange stiffness.

IV. RESULTS AND DISCUSSION

A. Spin waves and exchange stiffness

As an example, experimental FMR data for $Fe_{0.46}Pt_{0.54}$ are presented in Fig. 2(a) for two different polar angles θ between the external magnetic field and the sample normal, i.e., $\theta=0°$ and $\theta=90°$. In this graph, the first derivative of the absorption signal is shown as a function of the external magnetic field. Note that the sharp resonance lines around $\mu_0 H_{ext}=0.33$ T are caused by paramagnetic impurities in the MgO substrate. The strong shift in the resonance field that can be assigned to the resonant microwave absorption of the FePt film is mainly due to the shape anisotropy that favors a magnetization direction in the sample plane ($\theta=90°$). For $\theta=0°$ a second resonance line is visible at $\mu_0 H_{ext}\approx 1.12$ T with a lower intensity compared to the resonance of the uniform mode at $\mu_0 H_{ext}\approx 1.28$ T. The full angular dependence is shown in Fig. 2(b) as contour plot of the first derivative of the absorption signal as a function of external field value and polar angle. The absolute values of the gray scale intensities describe the amplitude of the first derivative of absorbed microwave power according to the gray scale shown in Fig. 2(a). From this plot it can be seen that the spin-wave resonance line is clearly detectable for $-10° < \theta < 10°$. From the resonance position at $\theta=0°$ the exchange stiffness was calculated according to Eq. (3) for all Fe_xPt_{1-x} films with their different compositions.

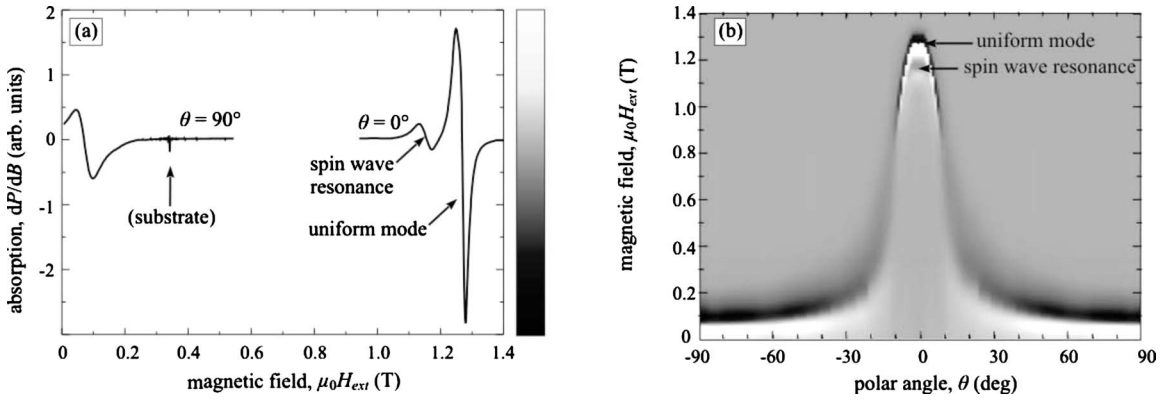

FIG. 2. (a) FMR spectra of epitaxial $Fe_{0.46}Pt_{0.54}$ at room temperature and $\nu_{rf} \approx 10$ GHz for two different angles between the external magnetic field and the sample normal. The first derivative of absorbed microwave power is plotted against the external magnetic field. (b) Contour plot of the first derivative of absorbed microwave power as a function of external magnetic field value and polar angle.

For comparison the exchange stiffness was also determined by means of the SPR-KKR method. For this purpose, the exchange constant of the coupling for Fe-Fe, Fe-Pt, and Pt-Pt pairs was calculated as a function of distance. This is shown in Fig. 3 for one example, i.e., $Fe_{0.46}Pt_{0.54}$. It is clearly visible that the exchange is dominated by the coupling between two nearest-neighbor Fe atoms. The coupling constant is about 14 meV yielding a ferromagnetic coupling. This value exhibits only a weak dependence on the composition in the range investigated in this work (not shown here). In the case of two neighboring Pt atoms or an Fe-Pt pair the exchange coupling is about one order of magnitude smaller. For next-nearest-neighbor Fe atoms the coupling prefers an antiferromagnetic spin arrangement, for third-nearest neighbors the coupling is ferromagnetic again. At distances above twice the lattice constant, the coupling constant (almost) vanishes. For the case of bcc Fe as a reference, an exchange stiffness of 24 pJ/m was calculated which is in good agreement to the experimentally obtained values of 21 and 25 pJ/m reported in the literature.[26,27] The values for the Fe_xPt_{1-x} system are summarized in Table I. Since there are various definitions of the exchange stiffness, for a better comparison the sum $A' = \Sigma_j J_{0j} r_{0j}^2$ in millielectron volt per angstrom is given in addition which is also sometimes called exchange stiffness in the literature. Again, the values of A' for all considered Fe-Fe, Fe-Pt, and Pt-Pt pairs were weighted by their probability and summed up. Its value is related to the exchange stiffness A as defined in this work by the inverse volume of the unit cell. Both experimentally and theoretically obtained values of the exchange stiffness are shown in Fig. 4 as a function of Fe content. In the experimental data, there is an increase in the exchange stiffness with increasing Fe content from 6 ± 4 pJ/m for $x=0.27$ to 15 ± 4 pJ/m for $x=0.67$. The results from SPR-KKR calculations are in good agreement to these values. The trend of increasing exchange coupling with increasing Fe content can be qualitatively understood in terms of both structural and compositional changes: the higher Fe content leads to a smaller lattice constant and therefore the exchange stiffness increases as can be seen from Eq. (4). However, this is only true for moderate changes in the lattice constants since large changes may change the value of the exchange coupling constant J significantly and may even yield an antiferromagnetic coupling. With respect to the compositional changes, by summing over all contributions of nearest-neighbor Fe and Pt atoms, the fraction of Fe-Fe contributions increases with increasing Fe content. Since these contributions are the ones with the highest exchange coupling, the exchange stiffness increases according to Eq. (4). For all compositions, the exchange stiffness is smaller than in bcc-Fe bulk material. Comparison with the value for FePt in the chemically ordered fct state reported in the literature, i.e., 10 pJ/m,[28] suggests that there is no measurable influence on the exchange

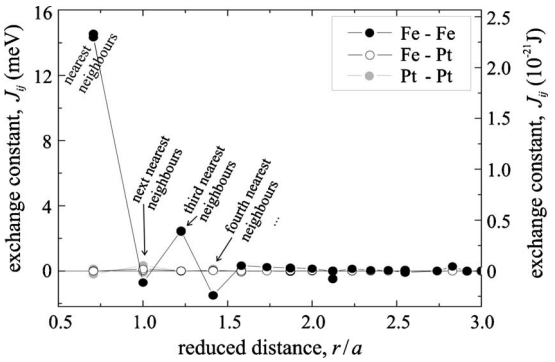

FIG. 3. Exchange coupling for Fe-Fe, Fe-Pt, and Pt-Pt pairs as a function of radial distance r in units of the lattice constant a.

TABLE I. Calculated and experimentally obtained values of the exchange stiffness. Note that the Fe contents of the measured samples slightly differ from the nominal values (cf. Fig. 4).

Fe content	A' (meV/Å)	A (pJ/m)	A_{exp} (pJ/m)
0.32	170	4.5	6.2 ± 4.0
0.40	320	8.7	11.4 ± 4.0
0.48	370	10.2	11.9 ± 4.0
0.60	400	11.5	10.3 ± 4.0
0.68	430	13.0	15.0 ± 4.0
0.72	470	13.9	

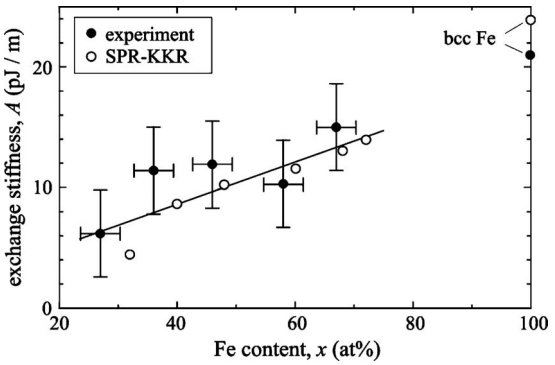

FIG. 4. Exchange stiffness in fcc-Fe_xPt_{1-x} films as a function of Fe content obtained by KKR calculations (open symbols) and FMR experiments at room temperature (filled symbols). The solid line is a guide to the eye. Experimental value for bcc Fe is taken from Ref. 26.

stiffness of the crystal symmetry in this case.

B. Magnetic anisotropies and exchange lengths

In order to calculate the exchange length, i.e., the width of a 180° domain wall, the magnetocrystalline anisotropy constant has to be known since the anisotropy energy and exchange coupling are competing values in this case according to the following equation for the exchange length assuming a Bloch-type domain wall:

$$\lambda_{xc} = \sqrt{A/K_4}, \tag{5}$$

where K_4 is the cubic fourth-order term of the magnetocrystalline anisotropy density (sometimes denoted as K_1 in the literature). In the case of our Fe_xPt_{1-x} films, the anisotropy constant was extracted from angular-dependent FMR measurements. Both polar and azimuthal angles were varied. In Fig. 5 the experimental FMR spectra are shown depending on the external magnetic field and azimuth angle as contour plot with the gray scale relating to the amplitude of the first derivative of absorbed microwave power similar to Fig. 2(b). The Fe content of the samples is increasing from the left to the right (27 at. %, 46 at. %, 58 at. %, and 67 at. % Fe). The decrease in the mean resonance field with increasing Fe content indicates the increase in the effective magnetization. In addition, the linewidth becomes smaller for higher Fe contents that may indicate an increase in relaxation times. However, a discussion of relaxation in FMR is beyond the scope of the paper. The magnetic anisotropy has been analyzed by the angular dependence of the resonance field which is plotted in Fig. 5 (lower panel). It is clearly indicating the fourfold anisotropy. Additionally, a twofold anisotropy contribution is visible. The easy direction of magnetization changes between $x=0.46$ and $x=0.58$ from the $\langle 111 \rangle$ directions to the $\langle 100 \rangle$ directions as it is known, e.g., for the composition-dependent magnetocrystalline anisotropy of Fe_xNi_{1-x} alloys. Also in the case of Fe_xPt_{1-x} alloys, changes in the easy direction of magnetization as a function of composition[20] and temperature[29] are reported.

In our case, the transition can be seen in Fig. 5 since for (a) and (b) maximum resonance fields are obtained for $\varphi = 0°$, 90°, 180°, and 270° whereas in (c) and (d) minimum resonance fields are obtained at these angles. Note that the twofold anisotropy contribution does not follow this trend: in all cases it is along a direction including an angle of 5° with the (100) direction of the substrate leading to a slight asymmetry in the angular-dependent resonance fields. This indicates an anisotropy due to steps of the substrate or may be growth induced. The latter seems to be a more likely explanation since the films are quite thick and therefore, substrate-

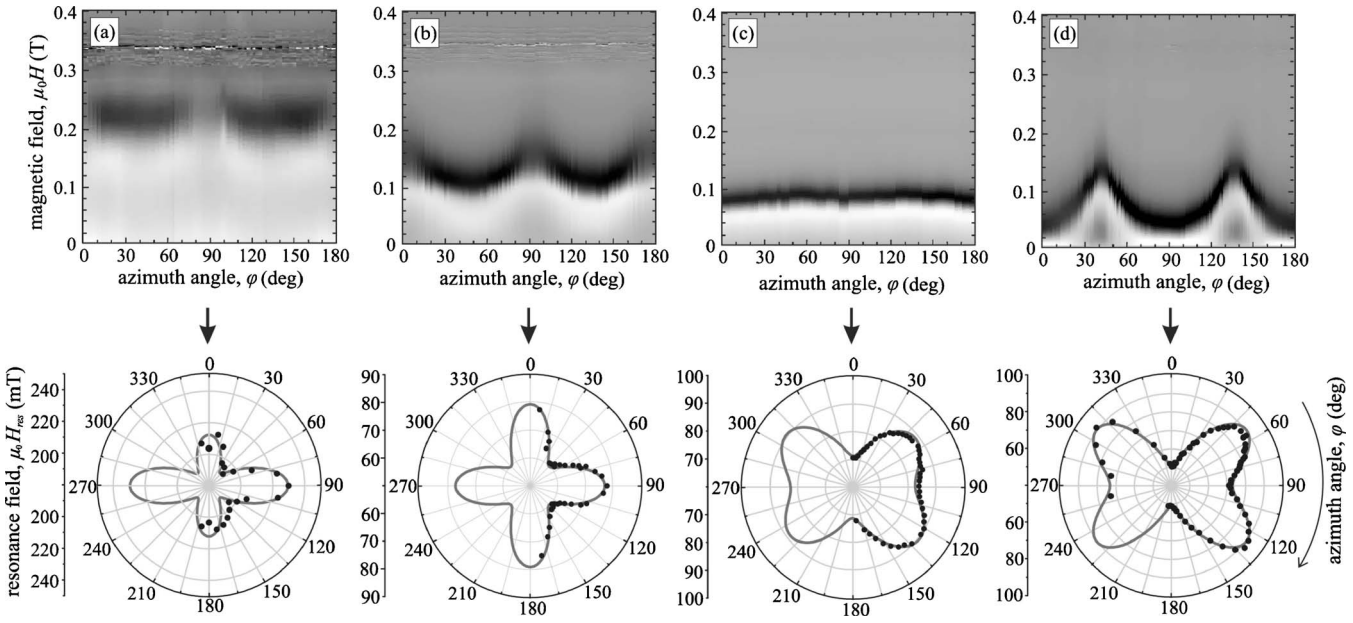

FIG. 5. Upper graphics: contour plot of the first derivative of absorbed microwave power as a function of external magnetic field value and azimuth angle of (a) $Fe_{0.27}Pt_{0.73}$, (b) $Fe_{0.46}Pt_{0.54}$, (c) $Fe_{0.58}Pt_{0.42}$, and (d) $Fe_{0.67}Pt_{0.33}$ at room temperature and $\nu_{rf} \approx 10$ GHz. Lower graphics: extracted azimuthal dependence of the FMR resonance field. Symbols refer to experimental data and lines refer to simulations.

induced anisotropies at the interface should not be measurable. However, its origin is not clear up to now but is of less importance since we will only roughly estimate the values of the exchange length.

The magnetocrystalline anisotropies were quantified by simulation of the azimuth and polar angle dependence of the resonance field using a program developed by Anisimov based on the Landau-Lifshitz-Gilbert formalism.[30] In this software, the resonance field is described in terms of minimization of the free-energy density including second- and fourth-order anisotropy contributions and the Zeeman energy.[31] The resonance field is calculated for any chosen pairs of polar and azimuthal angle, θ and ϕ, respectively, according to Ref. 32,

$$\left(\frac{\omega}{\gamma}\right)^2 = \frac{1}{M^2}F_{\theta\theta}\left(\frac{F_{\phi\phi}}{\sin^2[\theta]} + \frac{\cos[\theta]}{\sin[\theta]}F_{\theta}\right) - \frac{1}{M^2}\left(\frac{F_{\theta\phi}}{\sin[\theta]} - \frac{\cos[\theta]}{\sin[\theta]}\frac{F_{\phi}}{\sin[\theta]}\right)^2, \quad (6)$$

where $F_x(F_{xy})$ denotes the first (second) derivative of the free-energy density to the angle $x(xy)$. Both experimental polar and azimuthal angular dependence of the resonance field were fitted using the same set of fitting parameters, i.e., an effective magnetization, the spectroscopic splitting factor g, K_4 and in addition, a uniaxial anisotropy in the sample plane as discussed before. (The dependence on the polar angle is not shown here.) We obtained values of K_4 ranging between 2.8 ± 1.0 and 7.1 ± 0.5 kJ/m^3 for all compositions except $Fe_{0.58}Pt_{0.42}$. For the latter case, a smaller value of 1.6 ± 0.5 kJ/m^3 was found by simulation of the experimental data. This may be related to the transition of the easy direction of magnetization near that composition as mentioned above. All these values are rather small compared, e.g., to bulk Fe in the bcc state but of the same order of magnitude as in the case of pure Fe in the fcc state.[33]

Using the values of K_4 and the corresponding exchange stiffnesses, the exchange length is found to range between 40 and 50 nm for all compositions investigated in this work. This value is about twice the value of bulk bcc Fe [$\lambda_{xc} = 23.3$ nm (Ref. 27)].

V. CONCLUSION

By analyses of angular-dependent FMR and spin-wave resonance, the composition dependence of exchange stiffness, magnetocrystalline anisotropy, and exchange length in Fe_xPt_{1-x} films with compositions $0.27 < x < 0.67$ were determined. As the main result, the exchange stiffness constant was found to increase with increasing Fe content from 6 ± 4 to 15 ± 4 pJ/m. These values are in good agreement to the SPR-KKR results presented here. In addition, we found a clear indication of a transition of the in-plane easy direction of magnetization from ⟨111⟩ directions for Fe contents below the equiatomic composition to ⟨100⟩ for Fe-rich compositions. The exchange length calculated from exchange stiffness and magnetocrystalline anisotropy was about 40–50 nm and does not show any composition dependence within experimental errors.

Concerning the question raised in the introduction one may conclude that spin canting effects in chemically disordered Fe_xPt_{1-x} nanoparticles with diameters around 5 nm and below are unlikely since this diameter is only about a tenth of the bulk exchange length. In order to induce spin canting effects, the magnetic anisotropy of the nanoparticles would have to be 100 times larger than in the corresponding bulk material which was never observed.

ACKNOWLEDGMENTS

We thank M. Acet and H. C. Herper (U. Duisburg-Essen) for helpful discussions. This work was financially supported by the DFG within the framework of SFB 445.

[1] D. A. Allwood, G. Xiong, C. C. Faulkner, D. Atkinson, D. Petit, and R. P. Cowburn, Science **309**, 1688 (2005).
[2] T. Jourdan, F. Lançon, and A. Marty, Phys. Rev. B **75**, 094422 (2007).
[3] S. Bedanta and W. Kleemann, J. Phys. D **42**, 013001 (2009).
[4] S. Sun, C. B. Murray, D. Weller, L. Folks, and A. Moser, Science **287**, 1989 (2000).
[5] R. W. Chantrell, D. Weller, T. J. Klemmer, S. Sun, and E. E. Fullerton, J. Appl. Phys. **91**, 6866 (2002).
[6] B. Rellinghaus, S. Stappert, M. Acet, and E. F. Wassermann, J. Magn. Magn. Mater. **266**, 142 (2003).
[7] C. Antoniak, J. Lindner, M. Spasova, D. Sudfeld, M. Acet, M. Farle, K. Fauth, U. Wiedwald, H.-G. Boyen, P. Ziemann, F. Wilhelm, A. Rogalev, and S. Sun, Phys. Rev. Lett. **97**, 117201 (2006).
[8] D. K. Kim, D. Kan, T. Veres, F. Normadin, J. K. Liao, H. H. Kim, S.-H. Lee, M. Zahn, and M. Muhammed, J. Appl. Phys. **97**, 10Q918 (2005).
[9] H.-G. Boyen, K. Fauth, B. Stahl, P. Ziemann, G. Kästle, F. Weigl, F. Banhart, M. Hessler, G. Schütz, N. S. Gajbhiye, J. Ellrich, H. Hahn, M. Büttner, M. G. Garnier, and P. Oelhafen, Adv. Mater. **17**, 574 (2005).
[10] D. A. Garanin and H. Kachkachi, Phys. Rev. Lett. **90**, 065504 (2003).
[11] Y. Labaye, O. Crisan, L. Berger, J. M. Greneche, and J. M. D. Coey, J. Appl. Phys. **91**, 8715 (2002).
[12] H. Ebert, in *Electronic Structure and Physical Properties of Solids*, Lecture Notes in Physics Vol. 535, edited by H. Dreyssé (Springer, Berlin, 2000); H. Ebert *et al.*, The MUNICH SPR-KKR package, version 3.6, http://olymp.cup.uni-muenchen.de/ak/ebert/SPRKKR
[13] C. Kittel, Phys. Rev. **110**, 1295 (1958).
[14] C. Zener, Phys. Rev. **96**, 1335 (1954).
[15] S. D. Hanham, A. S. Arrott, and B. Heinrich, J. Appl. Phys. **52**, 1941 (1981).
[16] P. de V. du Plessis, J. Phys. Chem. Solids **32**, 1691 (1971).

[17] O. N. Mryasov, U. Nowak, K. Y. Guslienko, and R. W. Chantrell, Europhys. Lett. **69**, 805 (2005).
[18] C. Antoniak, J. Lindner, and M. Farle, Europhys. Lett. **70**, 250 (2005).
[19] W. Pepperhof and M. Acet, *Konstitution und Magnetismus des Eisens und seiner Legierungen* (Springer, Berlin, 2000).
[20] K. Adachi, D. Bonnenberg, J. J. M. Franse, R. Gersdorf, K. A. Hempel, K. Kanematsu, S. Misawa, M. Shiga, M. B. Stearns, and H. P. J. Wijn, in *Numerical Data and Functional Relationships in Science and Technology*, Landolt-Börnstein, New Series, Group III Vol. 19, Pt. A, edited by H. B. Landolt, R. Börnstein, and O. Madelung (Springer, New York, 1986), and references therein.
[21] C. Antoniak, M. Spasova, A. Trunova, K. Fauth, F. Wilhelm, A. Rogalev, J. Minár, H. Ebert, M. Farle, and H. Wende, J. Phys.: Condens. Matter **21**, 336002 (2009).
[22] W. B. Pearson, *A Handbook of Lattice Spacings and Structures of Metals and Alloys* (Pergamon, London, 1958), p. 535.
[23] A. I. Liechtenstein, M. I. Katsnelson, and V. A. Gubanov, J. Phys. F: Met. Phys. **14**, L125 (1984).
[24] J. F. Cochran, B. Heinrich, and A. S. Arrott, Phys. Rev. B **34**, 7788 (1986).
[25] Note that in the SPR-KKR package the definition of the exchange constant is different. It is based on the Heisenberg Hamiltonian written as $H_{xc}=-\Sigma_{i\neq j}J_{ij}\hat{e}_i\hat{e}_j$, where $\hat{e}_i$ and $\hat{e}_j$ are unit vectors pointing into the direction of the local magnetic moments. Thus, the absolute values of the moments (in units of μ_B) are already included in J_{ij}.
[26] P. Vavassori, D. Bisero, F. Carace, A. di Bona, G. C. Gazzadi, M. Liberati, and S. Valeri, Phys. Rev. B **72**, 054405 (2005).
[27] R. W. Gao, W. C. Feng, H. Q. Liu, B. Wang, W. Chen, G. B. Han, P. Zhang, H. Li, W. Li, Y. Q. Guo, W. Pan, X. M. Li, M. G. Zhu, and X. Li, J. Appl. Phys. **94**, 664 (2003).
[28] S. Okamoto, N. Kikuchi, O. Kitakami, T. Miyazaki, Y. Shimada, and K. Fukamichi, Phys. Rev. B **66**, 024413 (2002).
[29] O. Yamada, F. Ono, F. Arae, and H. Arimune, J. Magn. Magn. Mater. **15-18**, 569 (1980).
[30] A. Anisimov, simulation package *Cubic films*.
[31] C. Chappert, K. L. Dang, P. Beauvillain, H. Hurdequint, and D. Renard, Phys. Rev. B **34**, 3192 (1986).
[32] L. Baselgia, M. Warden, F. Waldner, S. L. Hutton, J. E. Drumheller, Y. Q. He, P. E. Wigen, and M. Maryško, Phys. Rev. B **38**, 2237 (1988).
[33] L. Albini, G. Carlotti, G. Gubbiotti, M. Madami,and S. Tacchi, J. Appl. Phys. **89**, 7383 (2001).